2024 6th International Conference on Reconfigurable
Mechanisms and Robots (ReMAR)
June 24-27, 2024. Chicago, IL, USA

A Novel Morphing Quadrotor UAV with Sarrus-Linkage-Based Reconfigurable Frame

Yan Wang, Chen Liu, Ketao Zhang[1]

2024 6th International Conference on Reconfigurable Mechanisms and Robots (ReMAR) | 979-8-3503-9596-9/24/$31.00 ©2024 IEEE | DOI: 10.1109/REMAR61031.2024.10619988

***Abstract*— Nature provides a repertoire of flyers demonstrating dynamic maneuvering during flight by effectively using their morphological changes, thus adapting to environmental variability. However, most conventional multirotor Unmanned Aerial Vehicles (UAVs) use rigid and single-configuration platforms, limiting their adaptability to environment and task changes. To address this limitation, this work proposes a novel morphing quadrotor UAV with a reconfigurable frame capable of changing its size during flight. The reconfigurable frame integrates two coplanar parallelogram four-bar linkages into each limb of a four-sided Sarrus linkage. This leads to a single degree of freedom (DoF) parallel mechanism with a symmetric structure, which ensures the four motor arms are coplanar and always with the same length while the morphing quadrotor UAV size changes. Based on this design, we investigate the feasibility of the morphing quadrotor UAV by building a proof-of-concept prototype that can change its size from a maximum of 410 mm to a minimum of 310 mm, meaning it can reduce the size by 24.4% and actively adapt to changing environment during flight. The in-flight morphing test shows that the morphing quadrotor UAV can implement a stable flight at various sizes. The experimental tests also demonstrate the potential for deploying the morphing quadrotor UAV in applications where the robot needs to navigate through narrow openings.**

I. INTRODUCTION

Multirotor UAVs and related technologies have been widely used for various applications, including search and rescue missions in extreme environments such as collapsed infrastructure following an earthquake or flood [1], [2]. These application scenarios require the multirotor UAVs to have better stability to resist external disturbances while exposed to strong winds. Meanwhile, the multirotor UAVs should also have good maneuverability and traverse ability, enabling them to enter damaged infrastructures through small gaps or narrow openings.

However, conventional designs of multirotor UAVs are based on rigid frames with fixed arms and shapes. This leads to challenges in deploying conventional multirotor UAVs with limited adaptability to the aforementioned application scenarios. Inspired by animal flyers, especially birds, researchers have developed novel morphing UAVs [3]–[6] by employing foldable/reconfigurable mechanisms in the body frame design to enable these UAVs to fold their wings [7] or rotor arms [8]–[18] or reconfigure their main frame [19]–[21], thus traverse some confined space. The morphing multirotor UAVs in the literature can be classified into two categories: (a) underactuated [8]–[21] and (b) fully actuated [22]–[27] according to the actuation scheme of the morphing multirotor UAVs.

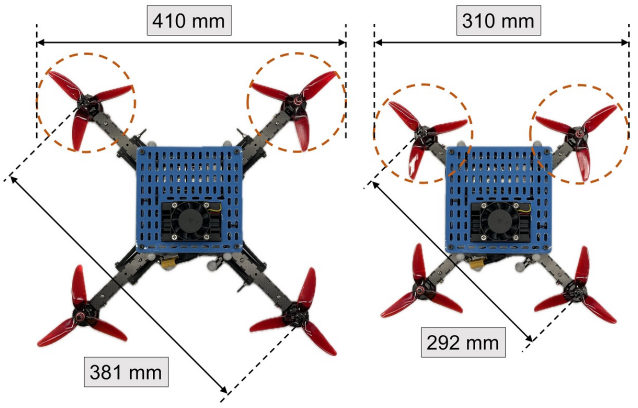

(a) The top view of the morphing quadrotor UAV.

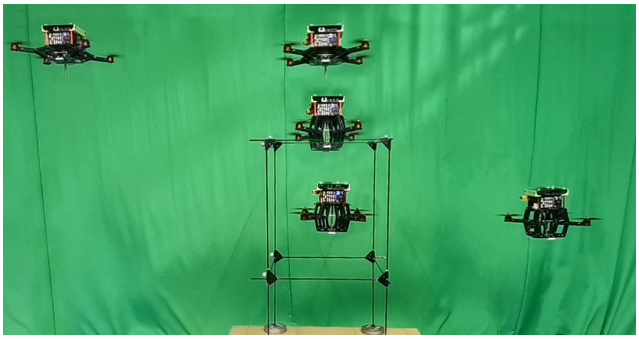

(b) The overlay of several snapshots of the morphing quadrotor UAV traverses the narrow carbon fibre frame.

Fig. 1. The novel morphing quadrotor UAV. (a) The top view of the morphing quadrotor UAV in the maximum and minimum sizes, respectively. (b) The process of the morphing quadrotor UAV traverses the narrow carbon fiber frame. From left to right. The morphing quadrotor UAV in the maximum size flies towards the carbon fiber frame. Then, it reconfigures the size to the minimum at the direct position above the carbon fiber frame. The morphing quadrotor UAV maintains the minimum size, vertically flies inside the carbon fiber frame, and then horizontally flies outside the carbon fiber frame.

Among the underactuated morphing quadrotor UAVs, there are mainly two design schemes, including the passively morphing quadrotor UAV [15], which resort to integrated elastic energy storage devices for shape morphing, and another type that utilizes actively actuated mechanisms to achieve the morphology change [8]–[14]. Most existing designs for morphing quadrotor UAVs adopted the latter design scheme to control the morphology change process effectively.

This work is partially supported by the Royal Society, International Exchanges Cost Share award EC\NSFC\211324.

[1]Y. Wang, C. Liu, and K. Zhang are with the Centre for Advanced Robotics, School of Engineering and Materials Science, Queen Mary University of London, UK (email: exx569@qmul.ac.uk, chen.liu@qmul.ac.uk, ketao.zhang@qmul.ac.uk)

Morphing quadrotor UAVs using multiple independent actuators to fold and unfold the motor arms have been developed in recent years. One of the typical examples is the foldable drone [14], which uses one servo motor per arm and can reconfigure to X, H, T, and O shapes by rotating its arms independently to adapt to different application scenarios. To guarantee the UAV stable flight at a specific size and safe morphing processes between different sizes during flight, this work also developed a control strategy to calculate the variation of the moment inertia matrix and the output of each motor in real-time. Yang et al. [8] designed a morphing quadrotor UAV that used four servo motors to synchronize the folding and unfolding motion of the four arms and maintain the symmetrical structure of the main frame during shape morphing, although the frame is a single DoF deformation mechanism. The foldable motor arm using scissor mechanisms connected in series generally has a large deformation ratio. However, the relatively complex structure with a large number of hinges is sensitive to accumulated manufacturing errors of the components. In contrast to the designs using multiple actuators, Tuna et al. developed a novel morphing quadrotor UAV termed Folly [11], [12] by employing a single DOF crank-slider linkage in each arm to rotate the motor arm around a shaft at the corner of the main frame instead of translation along arm axes passing through the geometric center. Along with this design principle, an origami-inspired foldable quadrotor UAV [16] was deployed using a thread-actuated mechanism that requires only one actuator. These existing designs show challenges in maintaining a symmetrical frame structure where multiple independent actuators are used to drive motor arms, though they enable more distinct shapes. In addition, the increased number of actuators requires more complex controllers to implement shape morphing during flight.

This paper presents a novel design for morphing quadrotor UAV consisting of a 1-DoF reconfigurable main frame that integrates two parallelogram 4-bar linkages into each limb of a four-sided Sarrus linkage. The two parallelogram 4-bar linkages, which share the motor arm as a common link, restrict the arm in the symmetric plane parallel to the upper and base platforms of the Sarrus linkage in all configurations. The symmetric four-sided Sarrus linkage enables the mainframe to retract and extend the four arms symmetrically using only one actuator. Based on the proposed design, a prototype of the morphing quadrotor UAV is built and a model-free cascade PID position controller is implemented for experimental tests to evaluate the performance of the new design scheme for the morphing quadrotor UAV.

The rest of the paper is organized as follows: Section II introduces the design of the novel reconfigurable frame, the system development of the morphing quadrotor UAV, and the control strategies. Section III details the morphing quadrotor UAV's performance characterization and experimental results. Then, we conclude our work in section IV.

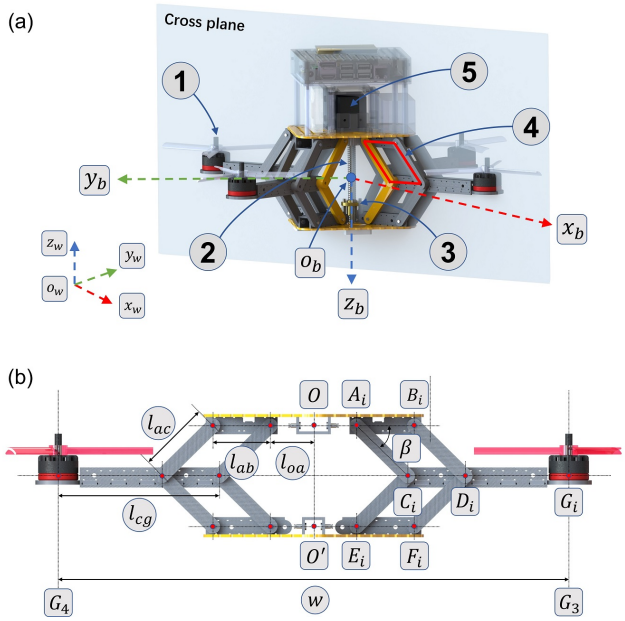

Fig. 2. The design scheme of the morphing quadrotor UAV. (a) 3D model of the morphing quadrotor UAV, which consists of the Sarrus linkage (the links highlighted in yellow) based reconfigurable frame and other essential components, including: 1. the electric motor (4 in total and the numbering of motors is based on the convention of PX4 [28]); 2. T8 lead screw; 3. the copper nut which is fixed to the base of the Sarrus-linkage; 4. the parallelogram 4-bar linkage; 5. the linear actuator (Dynamixel XM430-W210) for the Sarrus linkage. (b) The cross-section view of the morphing quadrotor UAV with the cutting plane, defined by axes of motors G_3 and G_4.

II. Design and System

This work develops a morphing aerial robot with a single-DOF reconfigurable frame, enabling robust in-flight size scalability and adaptability to various environments and tasks. This section provides a comprehensive account of the mechanical design and actuation scheme governing the reconfigurable frame and outlines the fabrication process for the novel morphing quadrotor UAV. Moreover, the control system for the new morphing UAV is introduced.

A. The Reconfigurable Frame

To achieve shape-changing, one of the essential characteristics of morphing UAVs, existing designs mainly focused on using foldable arms [8], [10]–[14] to reconfigure the position and orientation of the rotors either actively or passively. These designs generally require multiple actuators to fold and unfold the arms simultaneously. This leads to complex controllers for the reconfiguration process of morphing UAVs. To address such challenges, this work presents an alternative way of designing the morphing UAV structure by employing a reconfigurable mechanism as the main frame but with simple and rigid-bodied arms. Taking consideration of both the requirements for shape-changing and structural rigidity in various configurations, a range of deployable and reconfigurable mechanisms [29]–[31] were considered and the Sarrus linkage [31] is selected as the main frame given its symmetric structure and the single DoF

mobility. The 4-sided Sarrus linkage is an overconstrained parallel mechanism and requires only one actuator to drive the straight-line motion of the upper platform with respect to the base (highlighted plates in Fig. 2a). Two parallelogram four-bar linkages connected by revolute joints A_i, B_i, D_i and C_i, and E_i, F_i, D_i and C_i, respectively, are integrated into each limb of the 4-sided Sarrus linkage. The detailed design of the morphing quadrotor UAV is shown in Fig. 2, where the rotor base is denoted G_i. Taking the plane defined by axes of rotors G_3 and G_4 as the reference plane, the cross-section view of the morphing quadrotor UAV is shown in Fig. 2b. The symmetric structure of the Sarrus linkage constrains axes of the revolute joints C_i of all limbs to a common plane parallel to both the platform and the base in all configurations. The parallelogram four-bar linkages integrated into the *i-th* limb geometrically constrains the axis of the revolute joints D_i to the common plane. Under such geometry constraints, all rotor arms connected to joints C_i and D_i are constrained to the common plane and implement straight-line linear motion along two orthogonal lines when the Sarrus linkage changes its configuration. In addition, the axes of four rotors are perpendicular to the common plane in all configurations. This ensures that all rotor axes are parallel to each other without changing orientation during the shape morphing. As the rotor arms are symmetrically connected to the limbs of the reconfigurable frame, the 1-DoF Sarrus linkage is sufficient to convert the synchronized folding/unfolding motion of the limbs to the linear motion of the four motor arms connected to the limbs, resulting in size changes of the morphing quadrotor UAV. The size increases when the upper platform and the base of the Sarrus linkage move towards each other, and it decreases when the platform and the base move away from each other. In other words, reconfiguring the Sarrus-Linkage-Based frame leads to the size and shape change of the morphing quadrotor UAV.

As illustrated in Fig. 2a, the origin of the body coordinate frame o_b-$x_by_bz_b$ of the morphing quadrotor UAV is attached to the geometric center o_b, the x_b-axis and y_b-axis are in the common plane with x_b-axis coincides with the symmetric line of motor arms C_1G_1 and C_3G_3 and y_b-axis coincide with the symmetric line of motor arms C_1G_1 and C_4G_4. The world coordinate frame is denoted o_w-$x_wy_wz_w$.

The design parameters of the morphing quadrotor UAV include l_{ac}, length of the links A_iC_i, C_iE_i, B_iD_i, D_iF_i; l_{cg}, length of arms, C_iG_i; l_{oa}, the radius of the platform, OA_i; and l_{ab}, length of the links A_iB_i, C_iD_i, E_iF_i. With the above design scheme, the size w, the distance between G_3 and G_4 (or G_1 and G_2) of the morphing quadrotor UAV is calculated as

$$w = (l_{oa} + l_{ac} * \cos\beta + l_{cg}) * 2 \tag{1}$$

where β is the angle between link A_iC_i and the upper platform, i.e. the angle measured from A_iB_i to A_iC_i.

B. Actuation for the Reconfigurable Frame

Since the Sarrus linkage is a single DOF overconstrained mechanism that converts a rotary motion to a linear motion or vice versa, there are two ways to actuate the mechanism: 1) drive one of the articulated limbs using a rotary actuator, so the upper platform implements a linear motion with respect to the base; 2) use a linear actuator connecting the upper platform to the base thus to convert the linear motion to the rotary motion of links in the limbs. Considering the manufacturing tolerances of mechanical parts and the requirement for maintaining a symmetric structure of the morphing quadrotor UAV, the latter actuation approach is adopted in this work. As illustrated in Fig. 2a, the linear actuator is engineered based on the lead screw transmission principle. The T8 lead screw is connected to the shaft of the smart servo motor (Dynamixel XM430-W210), which is fixed to the upper platform. The copper nut of the linear actuator is connected to the base with a liner damper, which is used to prevent damage to the motor due to unexpected mechanical constraints of the overconstrained mechanism. The servo motor rotates the lead screw, thus driving the copper nut and the base to implement linear motion along the axis of the lead screw, which is perpendicular to both upper platform and base of the Sarrus linkage.

C. Electronic Components and Prototype

Based on the design and actuation scheme, a prototype of the morphing quadrotor UAV is developed and shown in Fig. 3. The electronic components for the morphing quadrotor UAV are listed in Tab. I. The Pixhawk 4 is employed as the flight controller with a built-in inertial measurement unit (IMU) to measure the morphing quadrotor UAV's acceleration and angular acceleration rate. Considering the reconfigurable frame and its lead-screw-based actuation scheme with the servo motor mounted at the center of the upper platform, the Pixhawk 4 is placed at the side of the servo motor and set the Autopilot Orientation as $ROTATION\_ROLL\_90$ in QGroundControl. Meanwhile, an offset of 30 mm for the inertial measurement unit (IMU) is set in $EKF2$ along the y-axis. The battery is placed on the other side of the servo motor to balance the mass distribution along the y_b-axis of the morphing quadrotor UAV. A NVIDIA Jetson Nano 4GB is used as the companion computer for installing the Robot Operating System (ROS), MAVROS and DynamixelSDK to control the UAV and the Dynamixel servo motors.

In this work, the reconfigurable frame of the morphing quadrotor UAV was fabricated by cutting carbon fiber panels using a CNC machine to minimize manufacturing errors. We used carbon fiber panels with 4 mm thickness for the limbs of the Sarrus linkage and panels with 3 mm thickness for the rotor arms. The width of the Sarrus limbs is 10 mm. The total weight of the morphing quadrotor UAV with all the electronic components is Approx. 1250 g, which is 40% of the total thrust provided by the rotors.

Considering the motion range of the linear actuator and the radius of the selected propellers, the values of the design parameters for building the prototype are set as follows: l_{ac} = 50 mm, l_{cg} = 112 mm, l_{oa} = 30 mm and l_{ab} = 40 mm. Substituting the above values into Eq. 1, it derives the maximum size from the shaft of the motor that is placed

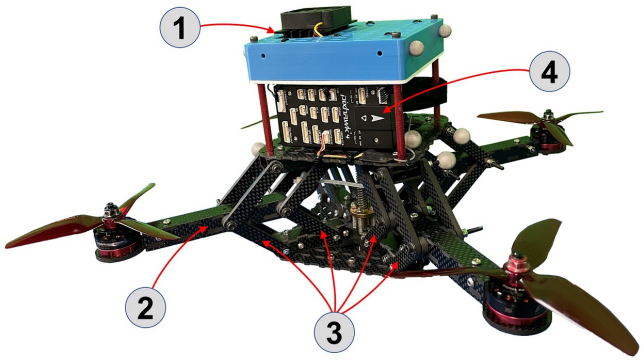

Fig. 3. The prototype of the morphing quadrotor UAV. 1. the onboard computer (NVIDIA Jetson Nano 4GB); 2. the arm; 3. the Sarrus limbs; 4. flight controller (Pixhawk 4).

in the diagonal is 384 mm when the frame is fully expanded (β = 0°) and the minimum size is 284 mm when the frame is fully contracted (β = 90°).

TABLE I

ELECTRONIC COMPONENT LIST

Module	Component	Manufacturer	Model
Propulsion module	Brushless Motor	EMAX	RS2205
	Propeller	HQProp	5×4.3×3
Control module	Flight Controller	HolyBro	Pixhawk 4
	Onboard Computer	NVIDIA	Jetson Nano 4GB
	RC Transmitter	RadioLink	AT9S Pro
	RC Receiver	RadioLink	R6DSM Receiver
other necessary module	Servo Motor	ROBOTIS	Dynamixel XM430-W210
	PDB	Matek	Mini Quad PDB
	Power Module	HolyBro	PM02
	Battery	Tattu	2000mAh 14.8V 120C 4S
	Converter	ROBOTIS	U2D2
	Gearing	RS component	100mm T8 Lead Screw & Copper Nut

The Sarrus linkage reaches its singular configuration when it is in the configuration where angle β = 90°. Further, physical interference between links constrains the reconfigurable frame's motion when it moves toward the fully expanded configuration. Hence, the prototype's angular displacement range of β is constrained to [15°, 85°] to avoid the singular configuration and physical interference. This means the distance between the upper platform of the base of the Sarrus linkage changes between 25.88 mm and 99.62 mm. It further derives from Eq. 1 that the size diagonal wheelbase w changes between 381 mm and 292 mm. In other words, the morphing quadrotor UAV can reduce its size (distance between the motor shaft in the diagonal position) by 23.3% from the maximum to the minimum.

D. Control System

To test the flight performance and validate the proposed design of the morphing quadrotor UAV, we adopted a model-free cascade PID position controller adapted from the PX4 [28], with the control law defined by Eq. 2. The general control structure is illustrated in Fig. 4. The definitions of parameters in Eq. 2 and Fig. 4 are listed in Tab. II.

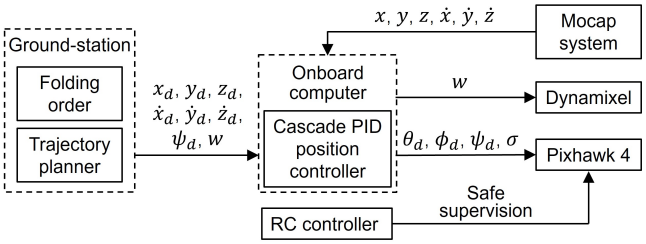

Fig. 4. The control structure of the morphing quadrotor UAV.

TABLE II

NOTATION DEFINITION OF THE CONTROL STRUCTURE

Notation	Definition
x, y, z	The current position of the morphing quadrotor UAV in the o_w-$x_w y_w z_w$ coordinate system of the flight testing space.
x_d, y_d, z_d	The desired position of the morphing quadrotor UAV in the o_w-$x_w y_w z_w$ coordinate system of the flight testing space.
ϕ, θ, ψ	The current pitch, roll, and yaw of the morphing quadrotor UAV in the body coordinate system of o_b-$x_b y_b z_b$.
ϕ_d, θ_d, ψ_d	The desired pitch, roll, and yaw of the morphing quadrotor UAV in the body coordinate system of o_b-$x_b y_b z_b$.
$\sigma \in [0,1]$	The desired throttle.
w	The desired size between the motor shaft in the diagonal position of the morphing quadrotor UAV.

$$\eta = k_p e + k_i \int_0^t e dt + k_d \dot{e} \tag{2}$$

where, $k_p, k_i, k_d \in \mathbb{R}^3$ are the controlling parameter vectors, $e \in \mathbb{R}^3$ represents the error between the desired and measured values, and $\eta \in \mathbb{R}^3$ represents the control output vectors..

Having the desired trajectory with the position x_d, y_d, z_d, velocity $\dot{x_d}, \dot{y_d}, \dot{z_d}$ and desired yaw angle ψ_d, generated by the Ground-station (Intel NUC) and the actual position and velocity of the morphing quadrotor UAV measured by a Motion Capture (MoCap) System installed in the flight testing space, the position and velocity errors are calculated as $e_p = [e_x, e_y, e_z]^T = [x - x_d, y - y_d, z - z_d]^T$ and $e_v = [e_{\dot{x}}, e_{\dot{y}}, e_{\dot{z}}]^T = [\dot{x} - \dot{x_d}, \dot{y} - \dot{y_d}, \dot{z} - \dot{z_d}]^T$, respectively. The messages from these devices communicate with the onboard computer via WiFi.

During the morphing process, the ground station (Intel NUC) publishes the desired w to drive the servo motor and reconfigure the Sarrus linkage-based frame, thus changing the size of the morphing quadrotor UAV.

III. EXPERIMENTS AND RESULTS

A. In-flight Morphing Test

To verify the feasibility of using the model-free cascade PID position controller for the morphing quadrotor UAV, we first test the morphing quadrotor UAV by tracking a circular trajectory $[x_d(t), y_d(t), z_d(t)]$ (as shown in Fig. 5) while the linear actuator actively driving the reconfigurable frame and changing the geometry size of the morphing quadrotor UAV during the flight. With the desired speed for tracking the trajectory, it takes 31.4 s for the morphing quadrotor UAV to complete a circular trajectory. The cycle for changing the morphing quadrotor UAV's geometry size

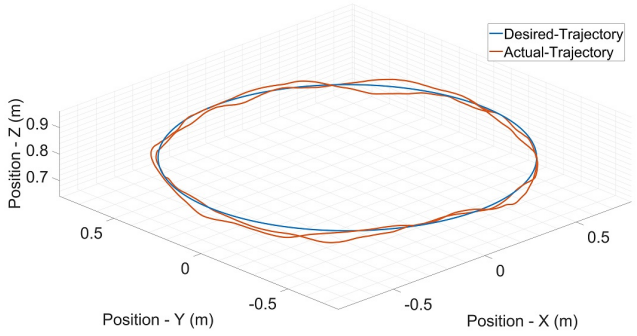

Fig. 5. In-flight morphing test. The morphing quadrotor UAV takes off at an arbitrary position of the flight testing space and then flies to the initial point $[0.75, 0, 0.8]$. Then begin to flight follow the desired trajectory: $t = 0 \sim 63$ s, $x_d(t) = 0.75 * cos(0.2t)$, $y_d(t) = 0.75 * sin(0.2t)$, $z_d(t) = 0.8$. Meanwhile, the servo motor (Dynamixel) unfolds the Sarrus mechanism to reconfigure the morphing quadrotor UAV's geometry size from the minimum to the maximum and then folds to the minimum. The geometry size change occurs four times during the whole process.

TABLE III

FLIGHT PERFORMANCE OF THE THREE EXPERIMENTS

Geometry size	μ [m]			σ [m]		
	x	y	z	x	y	z
Varied	0.028	0.046	0.013	0.004	0.005	0.001
Min	0.036	0.046	0.012	0.005	0.004	0.003
Max	0.017	0.031	0.012	0.002	0.001	0.001

from the minimum to the maximum and then to the minimum is 15 s. To collect sufficient data for systematic evaluation of the flight performance, the morphing quadrotor UAV flies two laps per flight and repeats the flight five times. At the trajectory's origin, the morphing quadrotor UAV is in its minimum geometry size. After 1.5 s, the morphing quadrotor UAV reconfigures to the maximum geometry size and then to the minimum. During the flight, the geometry size of the morphing quadrotor UAV implements four reconfiguration cycles, meaning the geometry size reaches the maximum and minimum four times, respectively. The batteries are fully charged, and the sensors of the morphing quadrotor UAV are calibrated before each flight test to avoid system errors. Fig. 5 shows one set of trajectory tracking data.

To further analyze the flight performance, the morphing quadrotor UAV is tasked to track the circular trajectory separately in the minimum and maximum geometry size, respectively. The average Root Mean Square Error (RMSE) is calculated to evaluate the trajectory tracking accuracy. Tab. III reports the mean μ and the standard deviation σ of the average RMSE in the x, y, z directions. The Varied, Min, and Max represent the state of the geometry size of the morphing quadrotor UAV in the varied, minimum, and maximum geometry sizes, respectively.

The average RMSE in Tab III indicates that the morphing quadrotor UAV in the maximum geometry size has higher trajectory tracking ability than it is in the minimum size. When the morphing quadrotor UAV implements in-flight morphing, the trajectory tracking accuracy is intermediate, referencing that in the maximum and minimum geometry size.

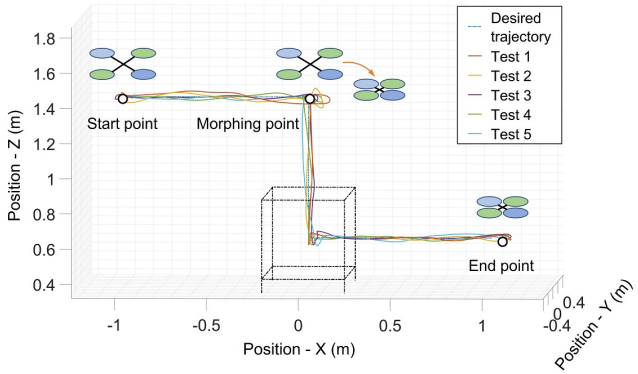

Fig. 6. The 3D trajectories of the morphing quadrotor UAV fly traverse the carbon fiber frame.

B. In-flight morphing to traverse the confined space

To illustrate the adaptability of the morphing quadrotor UAV, We first identified that the robot requires a minimum of 50 mm safety margin between the tip of the propellers and structures along the path to avoid any crashing through several flight tests using the morphing quadrotor in different geometry sizes. Since the maximum and minimum sizes (from propeller's tip-to-tip) of the UAV are 410 mm and 310 mm, as shown in Fig. 1a, the side lengths of corresponding square safety zones are 510 mm and 410 mm, respectively. To verify the morphing quadrotor UAV's adaptability to fly through horizontal and vertical openings and confined space, we designed and built a cuboid carbon fiber frame of which the horizontal opening is a square with a side length of 450 mm and the height of the vertical rectangle opening is 500 mm as a test rig (Fig. 1b), referencing these dimensions of the safety zone. During the test, four 300 mm bars are added to raise the frame to prevent the morphing quadrotor UAV from colliding with the ground while flying through the carbon fiber frame.

The location of the carbon fiber frame was obtained using the Mocap system with reflective markers attached to it. Given the position vectors of the frame's vertices in the Mocap system's coordinate frame, we designed a trajectory for the quadrotor UAV to track and fly through the openings and internal space of the frame.

To implement the passing-through flight tests, the morphing quadrotor UAV first takes off, then unfolds the Sarrus linkage to reconfigure the morphing quadrotor UAV to the maximum geometry size, then flies approach the start point $[-1.00, 0.00, 1.40]$ of the trajectory. It then moves towards the carbon fiber frame along a horizontal line 1.0 m over the top opening and reconfigures the morphing quadrotor UAV to its minimum geometry size at the point $[0.00, 0.00, 1.40]$. The morphing quadrotor UAV then descended along the vertical trajectory to pass the horizontal opening of the frame and hovered for 2 s at the center of the frame, then moved along the subsequent horizontal trajectory, passing the side vertical opening of the carbon fiber frame until reaching

the endpoint $[1.00, 0.00, 0.60]$. The morphing quadrotor UAV then landed on the right side of the frame.

The experiment results show that when the morphing quadrotor UAV moves close to the small openings, it can reconfigure its frame to the minimum geometry size and fly through the confined internal space of the frame without collision. Fig. 6 illustrates implemented 3D trajectories in five tests of the morphing quadrotor UAV passing through the carbon fiber frame. We also calculate the average RMSE to evaluate the trajectory error while passing through the carbon fiber frame. The mean μ of the average RMSE of the five experiments in the x, y, z directions and yaw angle ψ are 4.3 cm, 4.5 cm, 1.2 cm and 1.5°, respectively. The mean μ of the average RMSE further indicates that the 50 mm safe margin is essential for the UAV to fly without collision on the structure next to the flight path.

IV. CONCLUSIONS

This paper presented a novel morphing quadrotor UAV capable of reconfiguring its frame and changing the geometry size during flight. The new design integrated two parallelogram four-bar linkages into each limb of a four-sided Sarrus linkage to make a reconfigurable frame that requires only one actuator to move the four rotor arms synchronously, thus changing the UAV's size instead of using multiple actuators to drive length-changeable arms independently. A proof-of-concept prototype was built and tested in experiments designed to validate the key features of the morphing quadrotor UAV. The experimental results of the in-flight morphing and passing through confined space tests demonstrated that the new morphing quadrotor UAV can perform a stable flight even if the frame continuously changes its size in non-hovering flight. The morphing quadrotor UAV also demonstrated the advantage of passing through confined spaces by reconfiguring its geometry to the minimum dimension, which is impossible for a conventional UAV with a bigger dimension than the openings. With such reconfigurability and adaptability, the morphing quadrotor UAV can unfold its Sarrus-linkage-based frame towards the maximum geometry size for performing tasks requiring higher accuracy and fold its frame towards the minimum geometry size to navigate through narrow gaps and openings for operations in unknown environments. Future work will further investigate how changes in the moment of inertia of the reconfigurable frame affect flight performance and comprehensive control approaches for autonomous shape morphing in response to environmental changes.

REFERENCES

[1] J. Delmerico, S. Mintchev, A. Giusti, *et al.*, "The current state and future outlook of rescue robotics," *Journal of Field Robotics*, vol. 36, no. 7, pp. 1171–1191, 2019.

[2] M. Lyu, Y. Zhao, C. Huang, and H. Huang, "Unmanned aerial vehicles for search and rescue: A survey," *Remote Sensing*, vol. 15, no. 13, p. 3266, 2023.

[3] K. Patnaik and W. Zhang, "Towards reconfigurable and flexible multirotors: A literature survey and discussion on potential challenges," *International Journal of Intelligent Robotics and Applications*, vol. 5, no. 3, pp. 365–380, 2021.

[4] S. H. Derrouaoui, Y. Bouzid, M. Guiatni, and I. Dib, "A comprehensive review on reconfigurable drones: Classification, characteristics, design and control technologies," *Unmanned Systems*, vol. 10, no. 01, pp. 3–29, 2022.

[5] V. Riviere, A. Manecy, and S. Viollet, "Agile robotic fliers: A morphing-based approach," *Soft robotics*, vol. 5, no. 5, pp. 541–553, 2018.

[6] M. Zhao, T. Anzai, F. Shi, X. Chen, K. Okada, and M. Inaba, "Design, modeling, and control of an aerial robot dragon: A dual-rotor-embedded multilink robot with the ability of multi-degree-of-freedom aerial transformation," *IEEE Robotics and Automation Letters*, vol. 3, no. 2, pp. 1176–1183, 2018.

[7] D. Li, S. Zhao, A. Da Ronch, *et al.*, "A review of modelling and analysis of morphing wings," *Progress in Aerospace Sciences*, vol. 100, pp. 46–62, 2018.

[8] T. Yang, Y. Zhang, P. Li, Y. Shen, Y. Liu, and H. Chen, "Sniae-sse deformation mechanism enabled scalable multicopter: Design, modeling and flight performance validation," in *2020 IEEE International Conference on Robotics and Automation (ICRA)*, IEEE, 2020, pp. 864–870.

[9] N. Zhao, W. Yang, C. Peng, G. Wang, and Y. Shen, "Comparative validation study on bioinspired morphology-adaptation flight performance of a morphing quad-rotor," *IEEE Robotics and Automation Letters*, vol. 6, no. 3, pp. 5145–5152, 2021.

[10] D. Yang, S. Mishra, D. M. Aukes, and W. Zhang, "Design, planning, and control of an origami-inspired foldable quadrotor," in *2019 American Control Conference (ACC)*, IEEE, 2019, pp. 2551–2556.

[11] T. Tuna, S. E. Ovur, E. Gokbel, and T. Kumbasar, "Folly: A self foldable and self deployable autonomous quadcopter," in *2018 6th International Conference on Control Engineering & Information Technology (CEIT)*, IEEE, 2018, pp. 1–6.

[12] T. Tuna, S. E. Ovur, E. Gokbel, and T. Kumbasar, "Design and development of folly: A self-foldable and self-deployable quadcopter," *Aerospace Science and Technology*, vol. 100, p. 105 807, 2020.

[13] S. H. Derrouaoui, Y. Bouzid, M. Guiatni, I. Dib, and N. Moudjari, "Design and modeling of unconventional quadrotors," in *2020 28th Mediterranean Conference on Control and Automation (MED)*, IEEE, 2020, pp. 721–726.

[14] D. Falanga, K. Kleber, S. Mintchev, D. Floreano, and D. Scaramuzza, "The foldable drone: A morphing quadrotor that can squeeze and fly," *IEEE Robotics and Automation Letters*, vol. 4, no. 2, pp. 209–216, 2018.

[15] N. Bucki and M. W. Mueller, "Design and control of a passively morphing quadcopter," in *2019 International Conference on Robotics and Automation (ICRA)*, IEEE, 2019, pp. 9116–9122.

[16] D. Yang, S. Mishra, D. M. Aukes, and W. Zhang, "Design, planning, and control of an origami-inspired foldable quadrotor," in *2019 American Control Conference (ACC)*, IEEE, 2019, pp. 2551–2556.

[17] B. Li, L. Ma, D. Huang, and Y. Sun, "A flexibly assembled and maneuverable reconfigurable modular multirotor aerial vehicle," *IEEE/ASME Transactions on Mechatronics*, vol. 27, no. 3, pp. 1704–1714, 2021.

[18] P. Zheng, F. Xiao, P. H. Nguyen, A. Farinha, and M. Kovac, "Metamorphic aerial robot capable of mid-air shape morphing for rapid perching," *Scientific Reports*, vol. 13, no. 1, p. 1297, 2023.

[19] M. Zhao, T. Anzai, F. Shi, X. Chen, K. Okada, and M. Inaba, "Design, modeling, and control of an aerial robot dragon: A dual-rotor-embedded multilink robot with the ability of multi-degree-of-freedom aerial transformation," *IEEE Robotics and Automation Letters*, vol. 3, no. 2, pp. 1176–1183, 2018.

[20] M. Zhao, K. Kawasaki, X. Chen, S. Noda, K. Okada, and M. Inaba, "Whole-body aerial manipulation by transformable multirotor with two-dimensional multilinks," in *2017 IEEE International Conference on Robotics and Automation (ICRA)*, IEEE, 2017, pp. 5175–5182.

[21] B. Gabrich, D. Saldana, V. Kumar, and M. Yim, "A flying gripper based on cuboid modular robots," in *2018 IEEE International Conference on Robotics and Automation (ICRA)*, IEEE, 2018, pp. 7024–7030.

[22] D. Brescianini and R. D'Andrea, "Design, modeling and control of an omni-directional aerial vehicle," in *2016 IEEE international conference on robotics and automation (ICRA)*, IEEE, 2016, pp. 3261–3266.

[23] J. Y. Lee, K. K. Leang, and W. Yim, "Design and control of a fully-actuated hexrotor for aerial manipulation applications," *Journal of Mechanisms and Robotics*, vol. 10, no. 4, p. 041 007, 2018.

[24] M. Zhao, T. Anzai, F. Shi, X. Chen, K. Okada, and M. Inaba, "Design, modeling, and control of an aerial robot dragon: A dual-rotor-embedded multilink robot with the ability of multi-degree-of-freedom aerial transformation," *IEEE Robotics and Automation Letters*, vol. 3, no. 2, pp. 1176–1183, 2018.

[25] K. Kawasaki, Y. Motegi, M. Zhao, K. Okada, and M. Inaba, "Dual connected bi-copter with new wall trace locomotion feasibility that can fly at arbitrary tilt angle," in *2015 IEEE/RSJ International Conference on Intelligent Robots and Systems (IROS)*, IEEE, 2015, pp. 524–531.

[26] M. Kamel, S. Verling, O. Elkhatib, *et al.*, "The voliro omniorientational hexacopter: An agile and maneuverable tiltable-rotor aerial vehicle," *IEEE Robotics & Automation Magazine*, vol. 25, no. 4, pp. 34–44, 2018.

[27] P. Zheng, X. Tan, B. B. Kocer, E. Yang, and M. Kovac, "Tiltdrone: A fully-actuated tilting quadrotor platform," *IEEE Robotics and Automation Letters*, vol. 5, no. 4, pp. 6845–6852, 2020.

[28] D. Project, *Px4 user guide (main)*, [Online], `https://docs.px4.io/main/en/airframes/airframe_reference.html`.

[29] J. Patel and G. Ananthasuresh, "A kinematic theory for radially foldable planar linkages," *International journal of solids and structures*, vol. 44, no. 18-19, pp. 6279–6298, 2007.

[30] W.-a. Cao, S. Xi, H. Ding, and Z. Chen, "Design and kinematics of a novel double-ring truss deployable antenna mechanism," *Journal of Mechanical Design*, vol. 143, no. 12, p. 124 502, 2021.

[31] X. Song, H. Guo, Z. Deng, R. Liu, and B. Li, "Mobility analysis of a family of one-dimensional deployable mechanisms based on sarrus mechanism," in *2016 IEEE International Conference on Mechatronics and Automation*, IEEE, 2016, pp. 2265–2271.